Catena 160 (2018) 112–123

Contents lists available at ScienceDirect

Catena

journal homepage: www.elsevier.com/locate/catena

Importance of accessory minerals for the control of water chemistry of the Pampean aquifer, province of Buenos Aires, Argentina

Mélanie Vital[a], Damien Daval[b], Alain Clément[b], Sandra Quiroga[c], Bertrand Fritz[b], Daniel E. Martinez[a,*]

[a] Instituto de Geología de Costas y Cuaternario (UNMDP-CIC) – Instituto de Investigaciones Marinas y Costeras (CONICET-UNMDP), Mar del Plata, Argentina
[b] Université de Strasbourg/EOST, CNRS, Laboratoire d'Hydrologie et de Géochimie de Strasbourg, 1 rue Blessig, F-67084 Strasbourg Cedex, France
[c] Departamento de Química, Universidad Nacional de Mar del Plata, Argentina

ARTICLE INFO

Keywords:
Accessory minerals
KINDIS code
Pampean aquifer
Water chemistry control
Dissolution kinetics, modeling

ABSTRACT

The Pampean aquifer, in south east Argentina, is mainly constituted of loess-like sediments. These are clastic sediments mainly composed of quartz and aluminosilicates and calcrete concretions. Its hydrochemistry is generally studied assuming a chemical equilibrium between mineral phases and the aqueous fluids. The phases forming the matrix of this aquifer are considered to be the reactive phases responsible for the chemistry of the groundwater. In the present study, batch dissolution experiments were performed on calcrete and loess to better understand the source of the Pampean aquifer water chemistry and to measure the benefit of applying water-rock interaction models that use kinetic rate laws instead of thermodynamic equilibria. The different minerals composing the loess and calcrete samples were calculated using quantitative Rietveld refinement of X-ray powder diffraction (XRD) patterns. This analysis showed that the major phases of loess are quartz (~30 wt%) and feldspars (~70 wt%). The main components of calcrete are calcite (~95 wt%) and quartz (~5 wt%). Scanning electron microscopy with energy dispersive X-ray microanalysis (SEM/EDXS) was used to provide detailed information about the chemical composition of the powder samples, revealing the presence of traces of minerals like halite, barite and fluorapatite, which were not detected by XRD. The kinetic code KINDIS was used to carry out simulations using the minerals identified previously in their relative proportions to identify the signature of those geochemical phases on water chemistry. Experimental data from batch dissolution experiments were compared to simulated data. This investigation showed that water reached pseudo steady state concentrations due to the presence of fast dissolving phases like halite, barite, gypsum, plant phytolith. These phases appeared to be of major importance in controlling the chemical composition of the Pampean groundwater. Furthermore, this work showed that the KINDIS software can be used on all kinds of aquifers as it is very easy to modify the parameters of the simulation to adapt it to numerous situations. The modeling is a very important tool for thermodynamic and kinetic studies of groundwater chemistry; it enables the prediction of water quality and can help to understand the impact of anthropic or natural contamination on the groundwater.

1. Introduction

The Pampean aquifer exists in a large area (over one million km^2) in the geographical region of Argentina, known as Chaco-Pampean Plain (CPP). This aquifer is of major importance as it provides water for the population, agriculture and industry, which is related to 60% of the national gross domestic product (GDP) of the country (Schultz and Castro, 2003). The Pampean sediments are a series of sedimentary deposits; mainly silt, fine sand and clayed grain size, which are mostly of aeolian and fluvial origin and Upper Cenozoic age (Frenguelli, 1956). From a hydrogeological point of view, these sequences form an unconfined-semi confined aquifer system. It is constituted mainly by loess which is predominantly silt-sized clastic sedimentary rocks with approximately 20% of quartz and up to 70% of feldspars. Limestone (or calcrete) is also present from 2 to 4%. The occurrence of amorphous silica phases like volcanic glass or biogenic silica from plant phytoliths has also been extensively documented (Bundschuh et al., 2004; Bhattacharya et al., 2006; Borrelli et al., 2008; Borrelli et al., 2010; Martinez and Osterrieth, 2013; Osterrieth et al., 2015). In general, the soil composition is homogeneous, and most of its components originate from volcanic eruptions (Teruggi, 1957; Tricart, 1973).

The water of the Pampean aquifer has high concentrations of

* Corresponding author.
E-mail address: demarti@mdp.edu.ar (D.E. Martinez).

http://dx.doi.org/10.1016/j.catena.2017.09.005
Received 27 March 2017; Received in revised form 4 September 2017; Accepted 7 September 2017
Available online 21 September 2017
0341-8162/ © 2017 Elsevier B.V. All rights reserved.

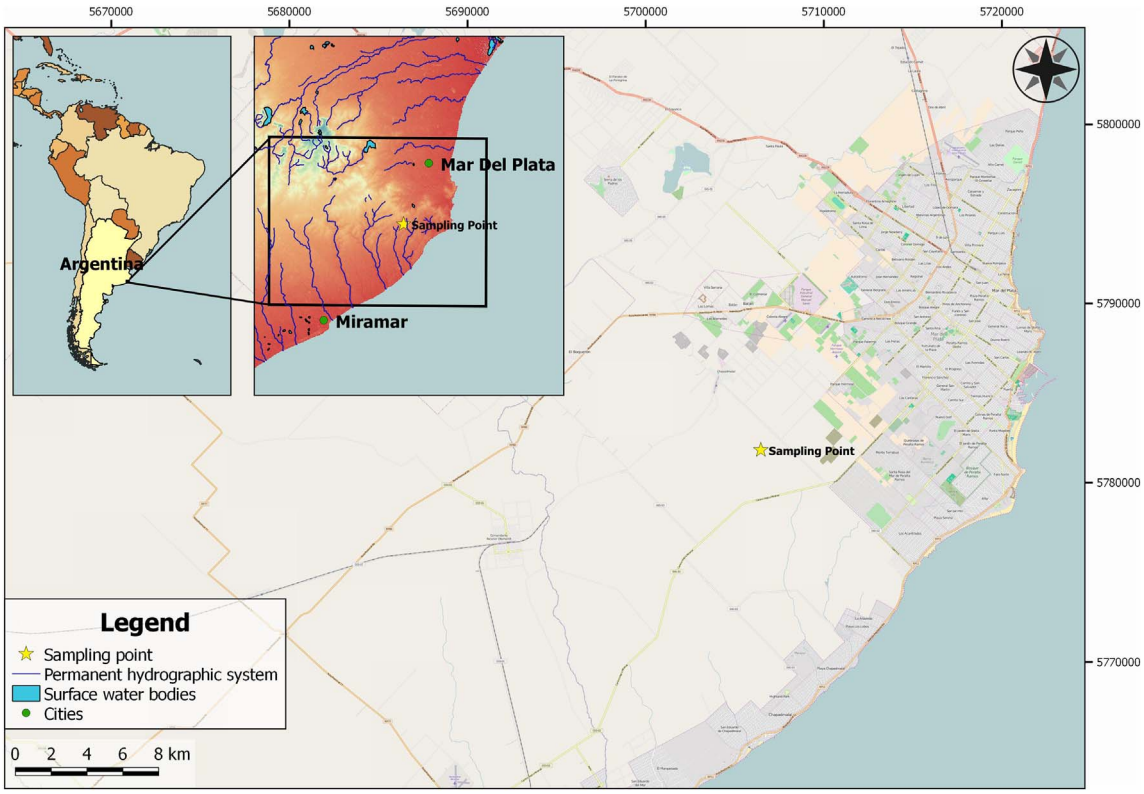

Fig. 1. Location of the studied area.

hydrogencarbonate, and sodium, with sodium being the dominant cation. The concentration of hydrogencarbonate varies between 300 mg/L to 700 mg/L and Na^+ concentration ranges from 50 to 250 mg/L. Ca^{2+} concentration is approximately 70 mg/L (Martínez and Bocanegra, 2002). Another characteristic of the Pampean aquifer is the elevated dissolved silica (SiO_2) concentrations which are approximately 65 mg/L (Martinez and Osterrieth, 2013). Some trace elements like barium (45 µg/L), and vanadium (50 µg/L), were also detected (Smedley et al., 2002). The groundwater quality varies greatly because of the presence of contaminants like fluoride, which is the monoatomic anion of fluorine F^-, and arsenic (Nicolli et al., 1989; Alarcón-Herrera et al., 2013). In the province of Buenos Aires, arsenic concentration can reach 23 to 289 µg/L (Al Rawahi et al., 2015), and fluoride concentration is about 1.0 mg/L (Martinez and Osterrieth, 2013), whereas in central Argentina arsenic and fluoride concentration can be as high as 4.8 mg L^{-1} (Bundschuh et al., 2004), and 28 mg L^{-1} respectively (Smedley et al., 2002).

Because of the major importance of the Pampean aquifer, its hydrochemistry has been studied for decades, in order to identify the processes that control the chemical composition of the groundwater, and to assess the evolution of water quality over time. Although modeling the water composition using geochemical codes implemented with dissolution/precipitation rate laws has already been extensively applied for limestone or sandstone aquifers (Nadler et al., 1980; Bullen et al., 1996; Mangeret et al., 2012; Antoniou et al., 2013), a similar approach on loess-like aquifers is currently missing, and is restricted to the modeling of processes such as adsorption dynamics (Chen et al., 2005; Huo et al., 2013). In fact, most of the previous studies aimed at understanding the groundwater composition of the Pampean aquifer were generally based on the chemical equilibrium theory (Logan et al., 1999; Martínez and Bocanegra, 2002; Glok Galli et al., 2014; Martinez et al., 2014; Zabala et al., 2015), which follows the usual perspective from the pioneering work of Garrels and Christ (1965). These studies indicate a dominance of silicates in the aquifer matrix composition, which are minerals with slow dissolution rates, making the equilibrium concept questionable. Nevertheless, this conceptual model strongly depends on fluid residence time, and the importance of silicate solubility has been demonstrated for some aquifers (Zhu, 2005; Zhu et al., 2006).

Therefore, the question is still pending for the Pampean Aquifer. One of the goals of this study is to go beyond the thermodynamic equilibrium approach and to introduce time-dependence of reactions to the understanding of geochemical processes.

Another purpose of this study is to unravel the origin of the chemical composition of the Pampean aquifer. The phases forming the solid matrix of this aquifer are considered to be reactive minerals and are used for hydro-geochemical interpretations. Other sedimentological or mineralogical studies, such as the pioneering work of Teruggi (1957) have stated the composition of this matrix. Few articles, where chemical equilibrium is considered, include determining the composition of the solution and the reactive phases (Martinez and Osterrieth, 2013; Dietrich et al., 2016). Minor fast-dissolving solids like salts or amorphous phases may play an important role in the evolution of underground waters in the Pampean aquifer. Also, few surveys considered the accessory minerals to study issues such as fluoride pollution (García et al., 2012; Borgnino et al., 2013), which could come from the dissolution of phases like volcanic glass (Nicolli et al., 1989; Gómez et al., 2009; Nicolli et al., 2012; Martinez et al., 2012). Another source of this contamination could be the release of fluoride originally co –precipitated with calcite (Kitano and Okumura, 1973); present as an impurity in limestone in the order of 220 µg/g (Garcia et al., 2006), or desorption from surface of oxides under alkaline conditions (García et al., 2014; Cury et al., 2015).

Overall, the aim of this paper is to shed light on the origin of the chemical composition of groundwater in the Pampean aquifer and to assess the use of water-rock simulations in this context, based on a kinetic assumption, using on laboratory experiments and/or field data.

2. Material and methods

2.1. Sample collection

Samples of calcrete and loess-like sediments were collected from an outcrop in the area of Mar del Plata in the province of Buenos Aires, Argentina ("S38°05′17. 27", "W57°39′14. 71") (Fig. 1). This area was chosen as being a representative area of the mineralogical composition of the Pampean aquifer in this sector of the Pampa plain. Furthermore, the outcrop includes both loess-like and calcrete sediments which were collected from a non-saturated zone with the same sedimentary composition as the Pampean aquifer. No treatment like rinsing was initially done on the samples used in the mineralogical investigations detailed in Sections 2.2, in order to preserve the soluble salts that can exist, such as ocean aerosols precipitated during dry periods in the non-saturated zone.

2.2. Mineralogical analyses

2.2.1. B.E.T reactive surface area

The specific surface area of the samples was measured using the Brunauer–Emmett–Teller (BET) methodology (Fagerlund, 1973). The analyses were performed on the calcrete and loess samples in the CINDECA laboratory, La Plata, Buenos Aires.

2.2.2. X-ray diffraction and Rietveld refinement

The mineralogical composition of calcrete and loess samples was characterized by X-ray diffraction (XRD). Sample preparation procedure consisted of grinding the rocks finely enough to make sure that the powder could be mounted so that there were as many random grain orientations as possible. Mineralogical analyses were carried out on each sample that was subjected directly to powder XRD study. Diffraction data were collected using a Bragg-Brentano diffractometer model D5000, from Bruker AXS, equipped with a copper anode (Cu Kα radiation). The conditions for generating the X-ray beam were 30 mA and 40 kV. Scans were taken for 2θ ranges from 3 to 65° with 0.03°/s steps, and a counting time of 25 s per step. Rietveld refinements were carried out with the program Fullprof (Rodríguez-Carvajal, 2001), following a standard procedure described in Daval et al. (2009). The refinement of calcrete was realized with calcium carbonates and quartz as the dominant phases. Calcium carbonates, quartz and albite phases were chosen for loess refinement. In brief, peaks were defined as being pseudo-Voigt with a variable percentage of Gaussian-Lorentzian character. The background consisted of 45 selected points with linear interpolation between them. Starting values for cell parameters, as well as atomic positions and atomic displacement parameters, were taken from previously published crystal structure refinements (Markgraf and Reeder, 1985; Levien et al., 1980; Prewitt et al., 1976).

A Lebail refinement with constant scale factor was first performed with the following steps: (1) the surface displacement and the zero delay of the goniometer parameters were refined, followed by (2) the refinement of the unit cell dimensions of the phases; (3) pseudo-Voigt mixing parameters were refined (η_0 and X), followed by the parameters (U, V, W and IG) of the modified Cagliotti function. This iterative procedure was stopped when the reduced χ^2 reached a minimum or became unstable. All the parameters were then fixed, subsequently permitting the Rietveld refinement, leading to refinement of scale factors and atomic positions of the major phases. The quality of the fit between the calculated and observed diffraction-profiles was evaluated using standard indices of agreement, such as the reduced χ^2 index defined by Rodríguez-Carvajal (2001).

2.2.3. SEM/EDXS

A conventional scanning electron microscope (TESCAN model Vega 2) equipped with an Energy Dispersive Spectrophotometer (Pegasus XM4) was used for X-ray microanalyses to identify mineral phases in the powder samples. The solid samples were sprinkled onto adhesive carbon tapes supported on metallic disks and put forward for analysis. Energy dispersive X-ray spectra of the particles were acquired and the characteristic X-ray emission intensities of the mineral-forming elements were measured.

2.3. Clastics and calcrete dissolution in batch experiments

Dissolution experiments were carried out using batch experiments. All experiments were performed in 50 mL polyethylene tubes with plastic screw caps. 2,5 g of crushed calcrete or loess were added into the tubes and filled up to 50 mL of deionized water (pH 5.7).

A fraction of the solid samples was initially rinsed three times with milliQ water and once with ethanol. On the other hand, non-rinsed samples were also prepared.

The reaction tubes were continuously agitated using a motorized orbital shaker table at about 200 rotations per minute. Batch experiments conducted on rinsed samples were run over different durations of time; ranging from 1 to 360 min. Samples were collected after 1 min, 3 min, 10 min, 30 min, 60 min, 180 min and 360 min. Dissolution kinetics measured on non-rinsed samples were collected by varying the contact time from 1 min to 1020 min. The first tube of the series was recovered after 1 min, while the 13th tube was recovered after 1020 min. The pH of the supernatant solutions was measured at each time. All experiments were run in triplicates. Aliquots of each suspension were obtained and filtered through 0.45 μm Millipore filters.

2.4. Chemical analyses of the water samples from batch experiment

Dissolved silica was analyzed by using the silicomolybdate complex colorimetric method described by Horwitz et al. (1970). For the present work, the zirconium/alizarin red S method of Meyling and Meyling (1963) was used to quantify fluoride concentration. Fluoride forms a complex with zirconium which is responsible for a decrease in absorbance. The colored zirconium/alizarin complex is destroyed and a colorless zirconium fluoride complex is formed. Finally, sulfate concentrations were measured by the turbidimetric method (Tabatabai, 1974). Absorbance was measured using a UV-VIS spectrophotometer BrabdBioTraza Model 752 set to detect silica at 640 nm, fluoride at 540 nm and sulfate at 420 nm.

A flame photometer, brand CrudoCamaño, supplied with interchangeable filters was used to determine the concentrations of aqueous Ca^{2+} and Na^{+}.

2.5. Numerical simulations with KINDIS software

2.5.1. Stability diagrams

The software KINDIS (KINetic of DISsolution) (Madé et al., 1994) was developed at the LHYGES (Laboratory of Hydrology and Geochemistry) in Strasbourg, France. It integrates kinetic rate laws for dissolution reactions and thermodynamic laws applied to aqueous chemical speciation calculations during water-rock interaction simulations. The chemical composition of the water samples measured in batch experiments was used for geochemical modeling with KINDIS.

Using the cation $[Na^{+}]$ and $[Ca^{2+}]$ to proton activity $[H^{+}]$ ratios, the measured compositions were plotted in stability diagrams (Khorzinskii, 1965). The construction of these diagrams was done by plotting the concentration of calcium or sodium as a function of the measured orthosilicic acid concentration using the equilibrium conditions at a given temperature against the formation of various secondary phases for precipitating from solution. Every point in the diagram corresponds to different contact time durations between the sample and the solution from the batch experiments.

2.5.2. Kinetic modeling

Simulations of dissolution kinetics were carried out with KINDIS. As

Table 1
Values of dissolution constant k used in KINDIS software.

	k (mol/m^2/year)		
	acid	neutral	basic
Calcite[a]	1.6×10^{7}	4.89×10^{1}	1.04×10^{4}
Quartz[a]	3.22×10^{-4}	3.22×10^{-7}	1.62×10^{-9}
Labradorite[a]	4.26×10^{-1}	3.88×10^{-4}	3.88×10^{-4}
Fluoroapatite[a]	5.68×10^{3}	3.15×10^{-1}	3.15×10^{-1}
Barite[a]	3.94	3.94×10^{-1}	3.94E-01
Halite[a]	1.92×10^{7}	1.92×10^{7}	1.92×10^{7}
Gypsum[a]	5.05×10^{4}	5.05×10^{4}	5.05×10^{4}
Fern phytolith[b]		1.21 10^{-4}	

[a] Values of k from Palandri and Kharaka (2004).
[b] Values of k from Fraysse et al. (2009).

described in Madé et al. (1994), the simplified equation used to simulate the dissolution rate of a mineral *m* in the KINDIS geochemical code can be written as:

$$v^{S}_{dm} = K^{pH}_{dm} S^{eff}_{m} a^{n}_{H+}(1 - Q_m/K_m)$$

where k_{dm}^{pH} is the constant of the apparent dissolution rate intrinsic to mineral *m* at a given pH [mol/m^2/year]; S_m^{eff} is the effective or reactive surface area at the mineral/aqueous solution interface [m^2/kg H2O]; $a_{H+}{}^{n}$ is the activity of the [H +] ions in the aqueous solution, where *n* is a real exponent with a generally positive value in acidic solutions, zero in neutral solutions and negative in basic solutions. $(1 - Qm/Km)$ relates the dissolution rate to the saturation index of mineral *m* in an aqueous solution, where *Qm* is the ionic activity product and *Km* is the thermodynamic equilibrium constant known for the given temperature and pressure conditions from the database THERMODDEM (Thermochemical and Mineralogical Tables for Geochemical Modeling), from the Bureau de Recherches Géologiques et Minières (BRGM). The parameters of the apparent dissolution rate intrinsic to mineral *m* at a given pH were taken from Palandri and Kharaka (2004) and Fraysse et al. (2009) (Table 1). The reactive surface area was obtained from the previously measured B.E.T surface area of loess and calcrete. The pH of 5.7, which corresponds to pure water in equilibrium with atmospheric CO_2 pressure, was considered the initial pH.

The simulations were first run with the minerals detected and quantified by XRD and Rietveld analyses performed on loess and calcrete samples and named Simulation 1 (Tables 3 and 4). When the minerals were only detected by SEM/EDXS and not XRD, their proportions were considered to be less than 2 wt% of the whole sample, corresponding to the estimated detection limit of the XRD analyses. The simulations named Simulation 2 were run with the minerals detected by XRD and SEM/EDXS in loess and calcrete. In a third simulation, the amount of each mineral was adjusted to fit the experimental data. Attempts of adjusting the results of the model to the experimental concentrations of silica were realized first by adding phases like biotite or plant phytolith, because Osterrieth and Martínez (1993) demonstrated that the latter phases are more altered than volcanic glasses and are probably responsible for the high concentration of silica in the Pampean aquifer. A second step to adjust the concentration of fluoride consisted of adding F-biotite or fluorite into the simulations and of modifying the nominal composition of calcite in the thermodynamic database of KINDIS, by including 0.1% of fluoride impurity. This value corresponds to the proportion of fluoride that could be present in calcite as an impurity (Kitano and Okumura, 1973; Garcia et al., 2006).

An ultimate set of simulations was run over 60 years, which is considered to be an average of the residence time of the Pampean aquifer (Martínez et al., 2016). Simulations with only the major minerals (detected by XRD) were compared to simulations including all the minerals and their proportions that were needed to fit the experimental data from batch experiments.

The software INFOSTAT (Di Rienzo et al., 2011) was used to calculate the Root Mean Square Deviation. This represents the sample standard deviation of the differences between calculated values and observed values. The best fit between the experimental data and the simulated data was obtained when the RMSD is close to 0.

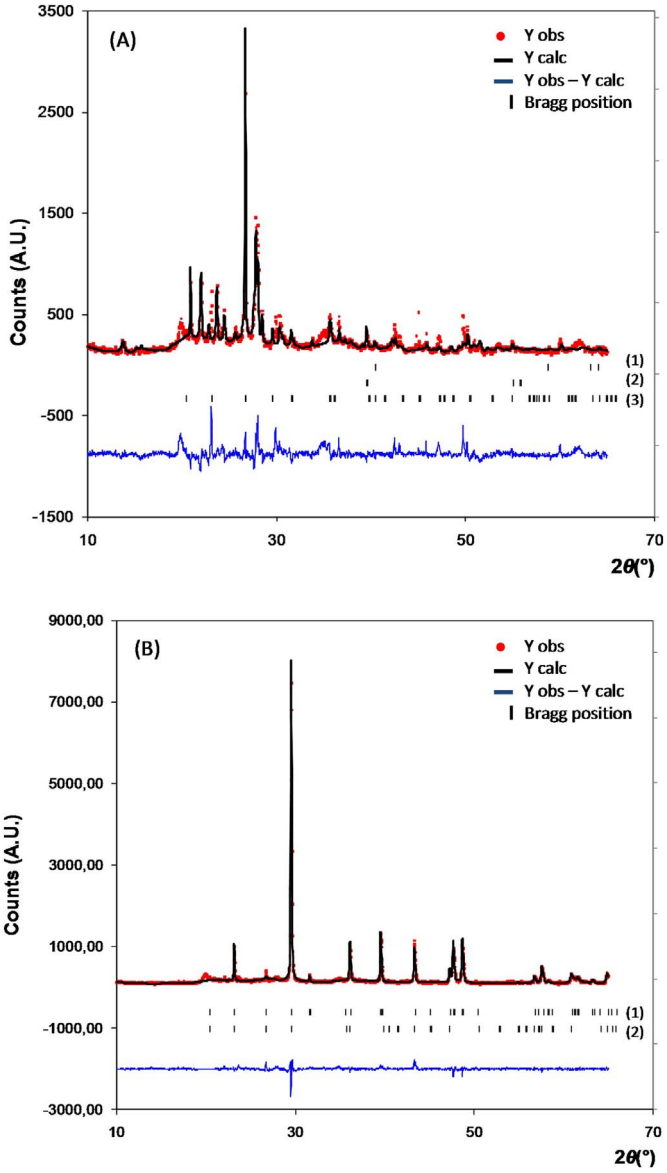

Fig. 2. Rietveld Best-fit matching for (A) loess (1) and (B) calcrete (1) samples. The red dots corresponds to the diffraction pattern from X-ray diffraction. The black line is the result of refinement with Rietveld. The vertical black lines correspond to the Bragg positions of (1) calcite, (2) quartz and (3) albite, respectively. (For interpretation of the references to colour in this figure legend, the reader is referred to the web version of this article.)

3. Results

3.1. Mineralogical analyses

3.1.1. B.E.T reactive surface area

The measured B.E.T reactive surface area of loess was 56.63 m^2/g ± 0.80 m^2/g and 41.73 m^2/g ± 0.11 m^2/g for calcrete (Vital et al., 2015).

3.1.2. X-ray diffraction and Rietveld refinement

The results of the Rietveld refinements represent the final output from each sample when the best possible fit had been achieved between

Table 2
Weight percentages of the different minerals in calcrete and loess samples calculated from Rietveld refinement of XRD patterns and overall goodness of fit (χ^2 value). Note that this value should approach 1.0 for a perfect fit between the measured and modeled patterns.

	Loess (1)	Loess (2)	Loess (3)	Calcrete (1)	Calcrete (2)	Calcrete (3)
	Wt%	Wt%	Wt%	Wt%	Wt%	Wt%
Calcite	0	0	0	98.70	94.91	94.61
Quartz	22.29	27.77	30.36	1.30	5.09	5.39
Albite	77.71	72.23	69.64	0	0	0
$\times^2$	5.74	5.55	5.86	3.93	3.97	3.49

the observed and calculated XRD patterns. The final output of the first samples of loess (A) and calcrete (B) can be seen in Fig. 2. The typical Bragg peaks for quartz at 2θ = 26.7° can be observed in Fig. 2A. The second highest peak at 2θ = 27.84° is representative of feldspars like albite. In Fig. 2B, calcite is detected with a characteristic peak at 2θ = 29.42° (Downs and Hall-Wallace, 2003). Importantly, the diffraction from crystalline substances is characterized by well-defined Bragg peaks in X-ray diffraction, whereas amorphous substances do not show sharp Bragg peaks. Consequently, the results obtained thereafter do not consider the amorphous biogenic phases or volcanic ashes that can be found in the Pampean aquifer and can constitute up to 30 wt% of the solid samples (Teruggi, 1957).

The results of the mineral quantification and an estimate of the overall goodness of fit of each analysis are provided in Table 2. In the crystalline part of the sample powders, quartz is found in all the samples ranging in abundances from 20 to 30% in loess and less than 6% in calcrete. The major components of loess are plagioclases like albite and represent over 70% of the samples. Calcite is present in significant proportions in calcrete (over 90%) but not detected in loess. The overall goodness of fit, expressed by χ^2, ranges from 3 to 6, indicating that the simulated patterns are in close agreement with the measured diffractograms.

3.1.3. SEM/EDXS

The SEM/EDXS provides information regarding the mineralogical composition of the samples based on chemical analyses. The analyses of loess samples allowed the identification of albite ($NaAlSi_3O_8$), and other plagioclases with various Ca^{2+}/Na^+ proportions, like labradorite, were also detected. SEM/EDXS characterization of calcrete confirmed the preponderance of calcium carbonates ($CaCO_3$). Halite (NaCl), barite ($BaSO_4$), (Fig. 3A), and fluorapatite ($Ca_5(PO4)_3F$), (Fig. 3B), were identified in both loess and calcrete samples.

3.2. Numerical simulation with KINDIS

3.2.1. Stability diagrams

The aqueous speciation was calculated with the KINDIS software in order to plot the results of the chemical composition of the water samples in contact with non-rinsed sediments, and estimate the stability of minerals against the solution composition. In general kaolinite and montmorillonite are the stable minerals pointing out the dissolution of plagioclase feldspars during batch experiments (Fig. 4), for which anorthite and albite represent the end-member feldspars. The horizontal line indicates the saturation with respect to calcite. The position of the line depends on the pCO_2. Here the pCO_2 has been considered as that of atmospheric levels ($10^{-3.5}$) which defines Log $(Ca^{+2})/(H^+)^2 = 13.02$ at equilibrium with calcite. Water samples of the batch experiment are generally very close to calcite saturation, showing that the solution reaches apparent steady-state values very quickly.

For both loess and calcrete, at 25 °C, the aqueous solutions are saturated with respect to quartz when $\log(H_4SiO_4) > -4$ and they become saturated with respect to both quartz and amorphous silica when $\log(H_4SiO_4) > -2.7$.

Again, the aqueous samples reached SiO_2 saturation within the first hour of reaction.

3.2.2. Dissolution kinetics of loess

The concentrations measured at each time in the batch experiments were represented as a function of time, both for the rinsed and non-rinsed samples (Fig. 5). In both cases, steady-state concentrations were reached within the first minutes of reaction. The pH of the solutions were 7.5 for the experiments conducted on rinsed samples, but lower than the 8.2 value observed for non-rinsed samples. The concentrations of calcium and sodium are also lower ($10^{-4.5}$ mol·L^{-1} of Ca^{2+} vs.$10^{-2.5}$ mol·L^{-1} for non-rinsed samples, and $10^{-3.2}$ mol·L^{-1} of Na^+ vs.$10^{-2.8}$ mol·L^{-1}). Fluoride concentrations increase up to $10^{-4.2}$ mol·L^{-1} in the experiments conducted on non-rinsed samples, whereas no fluoride was detected when the samples were rinsed. On the

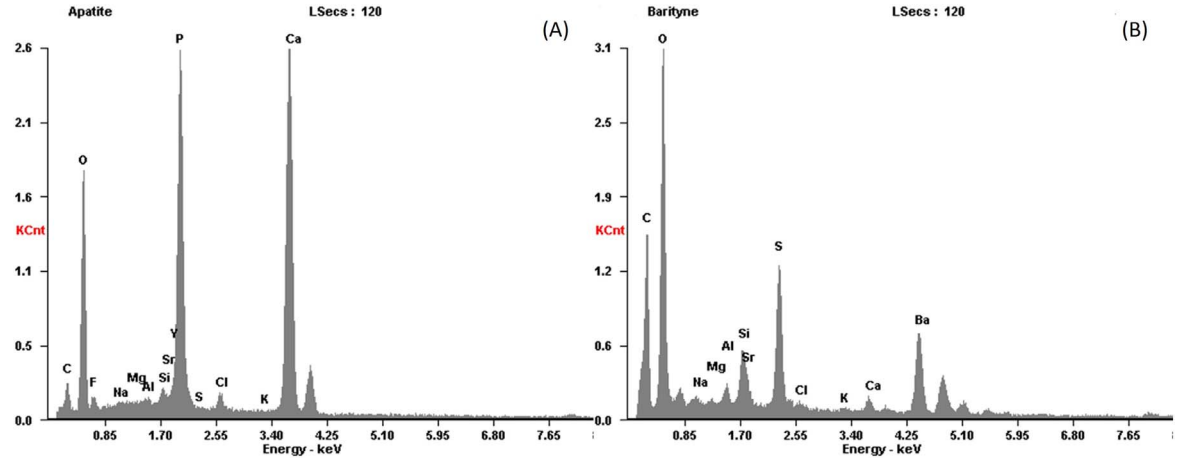

Fig. 3. SEM/EDS spectra of (A) fluorapatite and (B) barytine found in loess and calcrete.

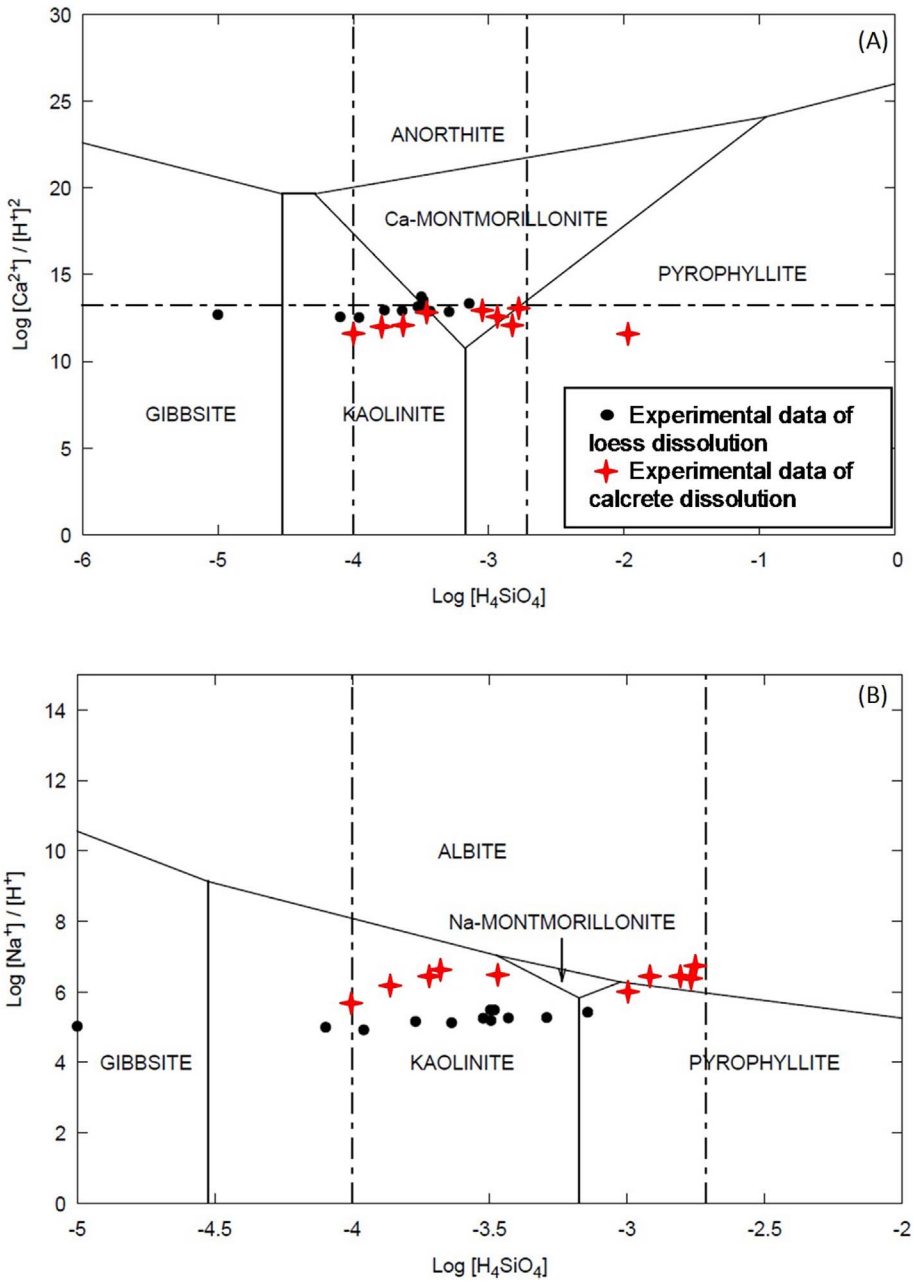

Fig. 4. Stability diagrams for the water samples from loess and calcrete dissolutions. The vertical lines indicate the limits of saturation of quartz and amorphous silica and the horizontal line represents the limit of calcite saturation.

contrary, the concentration of SiO_2 was not influenced by the treatment of the sediments. Sulfate values were up to $10^{-3.8}$ mol·L^{-1} in non-rinsed samples experiments, but it could not be detected in experiments conducted with the rinsed samples.

3.2.2.1. KINDIS simulations run using the results of Rietveld refinement. The results of experimental and simulated data obtained in this study were plotted as log (concentration) vs. time (Fig. 5). As a first test, Simulation 1 was realized with the results of Rietveld mineral quantification (i.e. 22.77% of quartz and 72.23% of feldspars like albite, see Table 3, Simulation 1). Note that the proportions of feldspars with varying chemical compositions are difficult to evaluate on the sole basis of XRD patterns. Although albite was chosen as a model mineral for the Rietveld refinement, SEM/EDXS observations revealed that plagioclase feldspars with various Na^+/Ca^{2+} ratios were present in the powder. Because of its intermediate chemical composition between the albite and anorthite end-members, the kinetic simulations were realized with labradorite, whose dissolution kinetics is intermediate to that of anorthite and albite, such that this approximation has only limited consequences on the results of kinetic simulations performed with KINDIS.

Strikingly, the modeled pH and concentrations of Na^+ are systematically underestimated compared to the measured concentrations in the batch experiments (Fig. 5). The modeled concentrations of Ca^{2+} are in good agreement with the concentrations measured for the experiments conducted on rinsed samples, but are at odds with the results obtained in experiments conducted on non-rinsed samples. Conversely, the concentration of SiO_2(aq) in the model is close to the experimental data.

3.2.2.2. Simulations run using the results from Rietveld refinement and SEM/EDXS analyses. To obtain a better fit of the experimental results, a dissolution simulation named Simulation 2 was realized, including the accessory minerals detected by SEM/EDXS. Barite, halite and fluorapatite were added in the simulation, considering that they represent 2% of the total sample weight each (Table 3, Simulation 2),

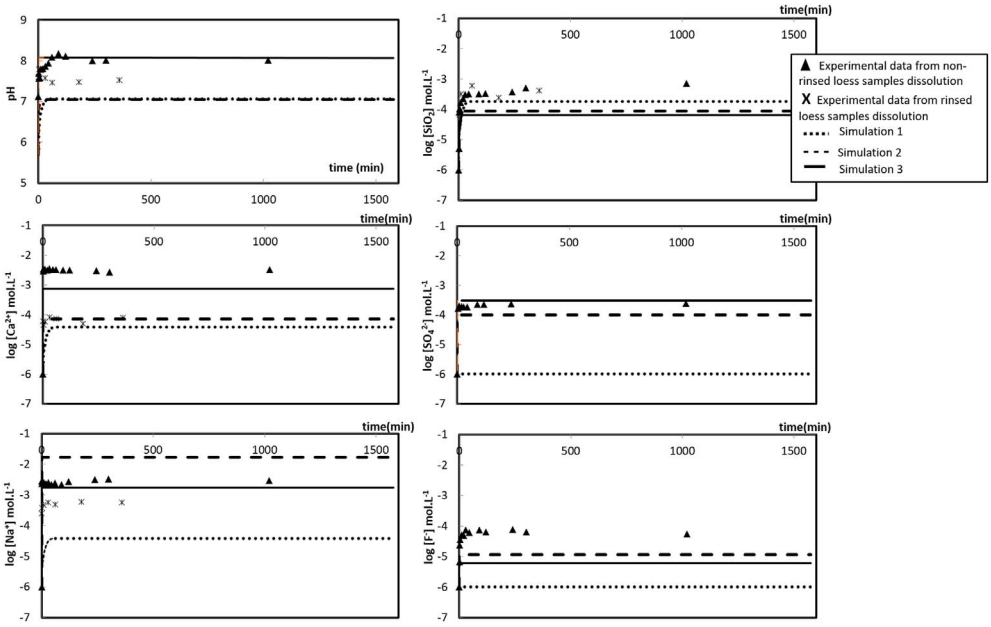

Fig. 5. Plot of the experimental concentration from batch dissolution of the loess sample and the simulated dissolution kinetics (simulation 1, Simulation 2, Simulation 3).

Table 3
Proportion of minerals for loess kinetic dissolution simulations in KINDIS software.

	Sim. 1	Sim. 2	Sim. 3
	Wt%	Wt%	Wt%
Quartz	27.77	24	27
Calcite			0.1
Labradorite	72.23	70	71
Halite		2	0.2
Gypsum			0.1
Barite		2	5×10^{-4}
Fluorapatite		2	2

which corresponds to the estimated quantification limit of our XRD apparatus. With the addition of 2% of halite, the simulated concentration of Na^+ increases and becomes higher than the experimental concentration of Na^+. Nevertheless, pH and equilibrium concentration values of Ca^{2+} and F^- are still lower than the experimental results of non-rinsed samples. When the simulation is run with 2% of barite, the concentration of sulfates is well fit but the concentration of barium is 10^{-4} mol·L^{-1}. Of note, Farías et al. (2003) and Smedley et al. (2002) measured the concentration of Ba^{2+} in the Pampean aquifer at around 10^{-6} mol·L^{-1}. Decreasing the proportion of barite in the simulation to reach natural conditions values leads to a decrease of sulfate concentration accordingly.

3.2.2.3. Fitting pH, sulfate and Ca^{2+} concentrations. To counter balance the effect of decreasing the proportion of barite, it may be necessary to add other sulfate-bearing minerals such as gypsum to model loess dissolution. Calcite must be added as well to increase the pH and calcium concentrations and to match the pH and Ca^{2+} concentration of non-rinsed samples. For the next step, simulations were run with the proportion of minerals indicated in Table 2 (Simulation 3). Those values were adjusted to obtain the best fits between the outputs of the numerical simulation and the concentrations measured experimentally in experiments run with non-rinsed sediments. The addition of calcite raised the pH and resulted in an increase of the simulated calcium concentration. Adding $CaSO_4$ increased the sulfate concentration. The addition of $CaCO_3$ and $CaSO_4$ resulted in a decrease of fluoride concentration. When the proportions of all minerals were adjusted in the model to match the experimental results, the steady-state concentration of SiO_2(aq) in the model decreased accordingly.

3.2.2.4. Fitting silica concentration. Martinez and Osterrieth (2013) showed that the dissolution of amorphous silica phases like silicophytoliths is responsible for the high concentration of dissolved silica in the water of the Pampean aquifer in the study zone. To the best of our knowledge, no rate data for the dissolution of the grass phytoliths, which represent the prevalent phytoliths of the Pampean aquifer, actually exists. Nevertheless, Fraysse et al. (2009) determined the dissolution rate of phytoliths extracted from fresh biomass of other representative plant species; therefore the rate of fern phytolith was chosen for this simulation. The measured silica concentrations from loess dissolution experiments were compared with the concentration of aqueous silica obtained with Simulation 3, corresponding to dissolution without phytoliths (Fig. 6). In Simulation 4, where the proportion of plant phytolith was raised to 10%, there was a stronger correlation between the simulated and the experimental data. On the other hand, adding biotite in the model meant that no adjustment could be made in order to match the experimental concentrations.

3.2.2.5. Fitting fluoride concentrations. Several tests were done to fit the outputs of the simulation to the measured concentrations of fluoride. A first step consisted of adding 2% of minerals like fluorite or F-rich biotite. Another way consisted of modifying the chemical composition of calcite in the thermodynamic database of KINDIS by adding a minor proportion of fluorine. Neither F-biotite and fluorite, nor the addition of calcite impurity could improve the agreement between modeled and the measured concentrations.

3.2.3. Dissolution kinetics of calcrete

The results of experiments conducted on rinsed and non-rinsed samples are shown in Fig. 7. The consequences of rinsing the samples resulted in lowering the pH (from 8.2 to 7.8) as well as the sodium concentration ($10^{-3.5}$ mol·L^{-1} vs 10^{-3} mol·L^{-1}). Also, the fluoride concentration in the experiments run with non-rinsed calcrete is close to$10^{-3.9}$ mol·L^{-1}, whereas no fluoride could be detected when the samples were rinsed.

3.2.3.1. KINDIS simulations run using the results of Rietveld refinement. To model the dissolution kinetics of calcrete, a first simulation was performed using the mineral proportions quantified

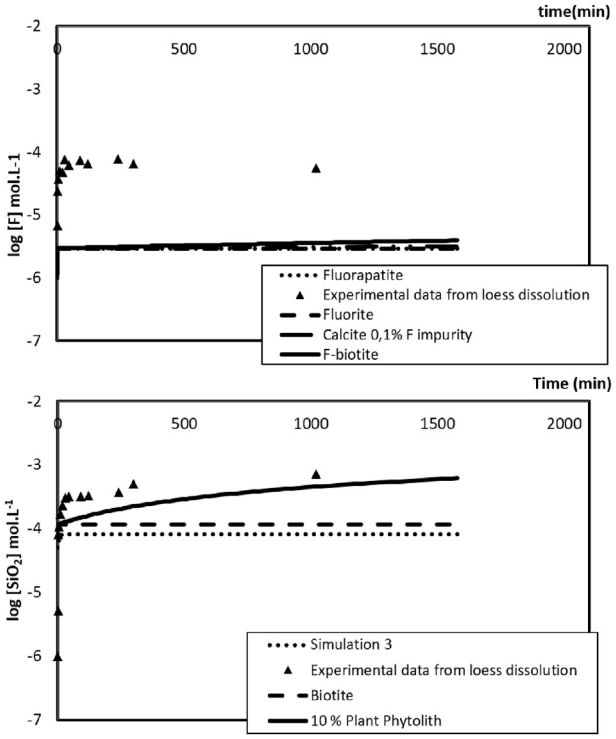

Fig. 6. Fitting of the fluoride and silica concentration from KINDIS kinetic simulation to the experimental results from loess batch dissolution.

by Rietveld refinement (Table 4, Simulation 1). Compared to the results obtained on non-rinsed samples, the simulation carried out with 94.61% calcite and 5.39% of quartz (Fig. 7) shows a strong agreement between the measured and modeled pH, but the simulated concentration of Ca^{2+} is overestimated, and the concentrations of Na^{+} and SiO_2(aq) are underestimated.

3.2.3.2. Simulations run using the results from Rietveld refinement and SEM/EDXS analyses. A second simulation was done including the minerals identified by SEM/EDXS (Table 4, Simulation 2). The addition of 2% of halite and 2% of fluorapatite did not improve the agreements between the outputs of the numerical simulations and the

Table 4
Proportion of minerals for calcrete kinetic dissolution simulations in KINDIS software.

	Sim. 1	Sim. 2	Sim. 3
	Wt%	Wt%	Wt%
Quartz	5.39	4	6
Calcite	94.61	92	89
Labradorite			2
Halite		2	0.2
Gypsum			0.5
Barite			5×10^{-4}
Fluoroapatite		2	2

experimental data, as the simulated concentrations of SiO_2, SO_4^{2-} and F^- remained much lower than the experimental data and the concentration of Na^+ is overestimated.

3.2.3.3. Fitting pH, sulfate and Ca^{2+} concentrations. A third simulation was performed to adequate the proportion of minerals in order to improve the agreement between the simulated and the experimental data (Table 4, Simulation 3). Barite was added in the model, but it was also necessary to add $CaSO_4$ to obtain sulfates in solution without increasing the Ba concentration too much. It can be seen from Fig. 7 that in this case, the concentration of calcium is too high and the concentrations of fluoride and silica are insufficient. Conversely, the simulated concentrations of sulfates and sodium are matching their experimental counterparts.

3.2.3.4. Fitting silica concentration. Like the loess sample, biotite and silicophytolith were added to the final reactants of the previous simulation (Fig. 8). The simulated silica concentration is closer to the measured concentration when adding 10% silicophytolith in the simulation of calcrete dissolution.

3.2.3.5. Fitting fluoride. The same methodology used for fitting fluoride in dissolution experiments run with loess samples was applied to fit the simulated results to the measured concentration of fluoride in experiments conducted on non-rinsed samples. Adding 2% of F-biotite, fluorite or 0.1% of fluoride as an impurity in the calcite mineral did not improve the agreement between the simulated and measured concentrations (Fig. 8).

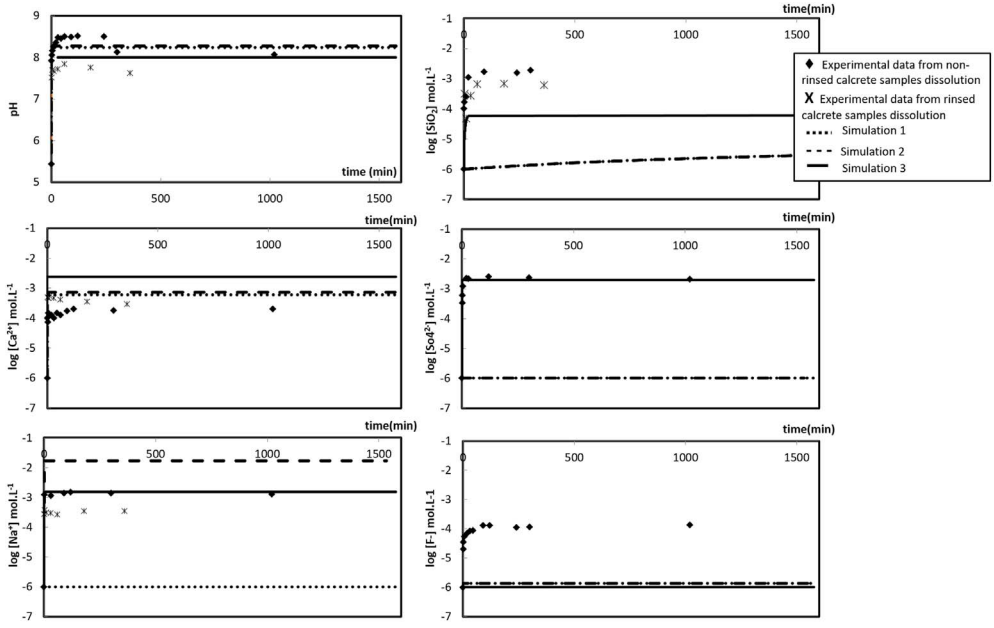

Fig. 7. Plot of the experimental concentration from batch dissolution of the calcrete sample and the simulated dissolution kinetics (simulation 1, Simulation 2, Simulation 3).

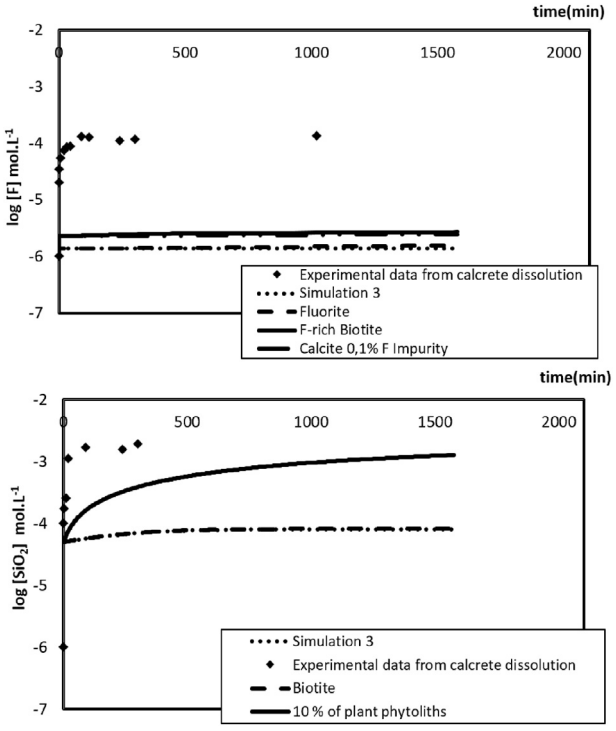

Fig. 8. Fitting of the fluoride and silica concentration from KINDIS kinetic simulation to the experimental results from calcrete batch dissolution.

3.2.4. Dissolution kinetics of the Pampean aquifer

As recent studies based on $^{3}H/^{3}He$ and CFCs monitoring estimated that the residence time for groundwater in the area is between 3 and up to more than 60 years (Martínez et al., 2016), batch simulations were performed with the KINDIS software over a 60 year-period. The first set of reactant phases included in the models was carried out on the major minerals detected in Simulation 1. Subsequently, all the minerals and their proportions needed to adjust the simulated data were used to perform additional simulations over 60 years. The modeled steady-state values for pH and concentrations were compared to the measured concentrations from wells taking water from the Pampean aquifer (Martinez et al., 2012). The results are shown in Table 5. If only major minerals are used, even after 60 years of simulation, the concentration measured in the Pampean aquifer could not be reached. Conversely, the simulation performed using the dissolution kinetics of accessory minerals yields similar results to measured data. Nevertheless, no simulations could manage to reach the fluoride concentration of the Pampean aquifer.

4. Discussion

4.1. Mineralogical analyses

The quantification of minerals by X-ray diffraction and Rietveld refinement showed that the main minerals of loess are feldspars (~70 wt%, here modeled as labradorite), and around 30 wt% of quartz. This result is consistent with the studies of Tricart (1973), Teruggi (1957) and Pye (1995), which reported that the main minerals in loess in Argentina,more precisely in the area of Mar del Plata, are plagioclases varying from 20 wt% to 65 wt%. These studies also evidenced that quartz is not very abundant, with a maximum proportion close to 30 wt%, but more frequently not exceeding 20 wt%. The main mineral found in calcrete is calcite (up to 95 wt%), but 1 to 5 wt% of quartz was also quantified by Rietveld refinement of XRD patterns. As mentioned above, for mixed materials, the estimated XRD detection limit is ~2 wt %, explaining why some minerals, like barite or fluorapatite, were not detected in the studied powders and could only be identified by scanning electron microscopy. Although Miretzky et al. (2001) attributed the presence of halite in the Pampean aquifer to a Holocene marine intrusion, it is more likely that the source of Na^+ and Cl^- is the dry and wet deposition of ocean aerosols, as Quiroz Londoño et al. (2012) measured Cl^- concentrations around 10 mg L^{-1} in rainwater in the area. Fluorapatite was considered to be present in many studies (Gómez et al., 2009; Pérez-Carrera and Cirelli, 2010; Martinez et al., 2012; Calvi et al., 2016); in contrast, only few studies evidenced the presence of barite in the Pampean aquifer (Borgnino et al., 2013).

4.2. Numerical simulation with KINDIS

4.2.1. Stability diagrams

The stability diagrams of the batch experiments showed that the final solutions after 5 h of reaction are present in the area of clays stability like Ca-montmorillonite, similar to some water samples from the Pampean aquifer (Martinez and Osterrieth, 2013). This observation suggests that the water chemistry in batch reactors after 5 h of reaction is similar to the chemistry of the groundwater. Because clays are known to be the stable secondary minerals, they were not included as possible dissolving minerals in the parameters for kinetics simulations. On the same footing, solutions are saturated with respect to amorphous silica, quartz and calcite.

4.2.2. Dissolution kinetics in batch experiments

The comparison of batch experiments realized with previous rinsing and no rinsing evidenced that this treatment removes the most reactive phases, such as halite and gypsum, resulting in a lower pH of the solution, a lower sodium concentration, and a lower calcium concentration for experiments conducted on loess.

The batch experiments and the simulations performed with the KINDIS software, whilst considering a kinetic approach of dissolution processes, demonstrate that the observed compositions cannot be derived by considering a thermodynamic equilibrium with only the major minerals. Instead, accessory minerals detected by SEM/EDXS had to be included in the models to reach similar concentrations of anions and cations. The studies using KINDIS of the dissolution of loess showed that the pH of the solution increased as a function of time when reacting with quartz and feldspars. The reactions of feldspar dissolution involve $[H^+]$ consumption, which explains the increase in pH of the final solution (Oelkers and Schott, 1995). Still, it was necessary to add 0,1 wt% of calcite in order to fit the simulated pH to the measured experimental

Table 5
Water chemistry of the Pampean aquifer compared to the results of KINDIS simulation with and without accessory minerals over 60 years.

	pH	LOG [Al][a]	LOG [Na^+][a]	LOG [Ca^{2+}][a]	LOG [F^-][a]	LOG [Si][a]	LOG [SO_4^{2-}]	LOG [Cl^-][a]
Pampean Aquifer	7.50	− 4.13	− 2.26	− 2.82	− 4.50	− 2.99	− 3.63	− 2.56
Loess (major + accessory)	7.76	− 4.70	− 2.36	− 3.12	− 5.60	− 2.70	− 3.61	− 2.36
Loess (major)	7.02	− 4.00	− 4.47	− 4.47	− 6.00	− 3.70	− 6.00	− 5.41
Calcrete (major + accessory)	7.41	− 5.27	− 2.69	− 2.61	− 5.60	− 3.71	− 2.69	− 2.70
Calcrete (major)	8.23	− 6.00	− 6.00	− 3.20	− 6.00	− 3.98	− 6.00	− 5.23

[a] Log concentration mol/L.

pH resulting from the formation of hydrogencarbonate ions that consume protons as well. The addition of calcite also caused the increase in the Ca^{2+} concentration, but not sufficiently. Consequently, gypsum was also added to the reacting mineral phases. Gypsum could not be detected by X-ray diffraction or by electron microscopy in the studied sample. Yet, some studies revealed the presence of gypsum in the Pampean aquifer (Quiroz Londoño et al., 2008; Dangavs and Blasi, 2002). The simulation that was carried out with the addition of 2 wt% of barite overestimated the aqueous concentration of barium; therefore it was necessary to add gypsum in the model, so that the sulfate concentration in the simulation matched the experimental data. The increase of Na^{+} in the first simulation could be explained by labradorite dissolution. Nevertheless, including 0.2 wt% of halite in the simulation parameters provided a much better agreement with the results of batch experiments, emphasizing the importance of this accessory mineral. Finally, raising the percentage of fluorapatite to 2 wt% in the model did not increase the concentration of fluoride in solution, which was always lower than the experimental concentration. García et al. (2012) considered the weathering of F-rich biotite as the most important and representative source of dissolved F^{-} in the groundwaters from the Sierras Pampeanas of Cordoba. Our dissolution kinetic simulations provided an original method to assess this suggestion: by adding in the simulations, minerals like fluorapatite, F-rich biotite and fluorite in proportions compatible with our mineralogical characterizations, it was not possible to reach the fluoride concentrations that were measured in the experiments. The experimental data could not be matched by modifying the calcite mineral or by adding trace amounts of fluoride. Because no fluoride was detected when the samples were previously rinsed, and because it was demonstrated above that fluoride cannot come from the dissolution of an F-rich accessory mineral, we suggest that the rapid release of fluoride (within a few seconds of reaction) results from its desorption from one or several minerals of the solid samples. This suggestion agrees with Borgnino et al. (2013), who indicated that fluoride is mostly released through its desorption from Fe-oxides under alkaline conditions.

To simulate the dissolution of calcrete, adding accessory minerals like halite, fluorapatite and gypsum was also necessary in order to match with the experimental data. However, the simulated concentration of Ca^{2+} was higher than the observed concentration, possibly revealing cationic exchange reactions during batch experiments.

In loess and calcrete dissolution experiments, the addition of amorphous silica phases was required to raise the SiO2(aq) concentration of the solutions. The addition of only 10 wt% silicophytolith to the reacting phase in the model improved the agreement between simulated and measured SiO2(aq) concentrations. This seems realistic, as silicophytoliths are abundant in the loess-like sediments in the area (Borrelli et al., 2010; Osterrieth et al., 2014, 2015). Therefore, the elevated aqueous silica content of the Pampean aquifer may be explained by the dissolution of silicophytolith.

4.2.3. Dissolution kinetics of the Pampean aquifer

The application of the equilibrium concept in former studies on groundwater (Martínez and Bocanegra, 2002; Glok Galli et al., 2014; Zabala et al., 2015) is mostly supported by the assumption of large residence times of groundwater, i. e., large contact time between the solution and the mineral phases with little to no renewal of the underground water. Nevertheless, simulations realized only with primary minerals did not result in a chemical composition similar to that of the Pampean aquifer water.

The simulation that was performed by applying the mineral assemblages, including accessory minerals, in batch experiments over a duration close to the residence time obtained for groundwater in the area as determined by Martinez et al. (2012) provides a satisfactory fit to the measured composition and validates, in that sense, the expected dissolution kinetics of the Pampean aquifer. Steady states concentrations were reached quickly due to the fast dissolution of accessory phases. The predicted values of Al^{3+} in the simulation over 60 years and the measured concentration of aluminum in the Pampean aquifer are very similar, revealing that the proportions of plagioclase in the input parameters were well defined. Moreover, the observed and simulated sodium and chloride concentrations are close, evidencing the importance of halite for the water salinity. Most of the studies on the chemistry of the Pampean aquifer in the region (Martínez and Bocanegra, 2002; Quiroz Londoño et al., 2008; Glok Galli et al., 2014; Zabala et al., 2015) showed a spatial distribution of hydrogencarbonate, sulfate, silica and fluoride which is homogeneous or non-increasing in the direction of the flow. This is consistent with the obtained results, from which it is possible to infer that the pseudo steady state concentrations are reached a few hours after recharge and that changes can be related to mixing, local recharge and lithologic changes. On the other hand, an increase of the chloride and sodium ions along the flow path is observed in the field, which is usually explained by cation exchange and the dissolution of halite.

The mineral assemblage including trace of fluorine impurity, F-rich biotite, fluoroapatite or fluorite used for the simulation of 60 years did not allow concentrations to reach the experimental fluoride concentrations, thus confirming the hypothesis of its desorption from primary minerals such as Fe-oxides.

5. Conclusion

The main mineralogical composition of the loess-like sediments forming the Pampean Aquifer in the Southeast of the Buenos Aires province was already known, and many hydrochemical models based on equilibrium concepts, have been used to explain the water chemistry. Nevertheless, a new approach demonstrates the importance of a detailed mineralogical description and the application of kinetic modeling to better define the minerals that control the chemical composition of the pore water.

X-ray diffraction has been shown to fail to get a complete scheme of the mineralogical composition of the sediments. Further SEM/EDXS investigations allowed determining the presence of important accessory minerals. The predominant minerals in the loess sample are quartz and feldspars. However, accessory minerals like halite, barite and fluorapatite were also detected by SEM/EDXS. In calcrete, calcite and quartz were found with trace amounts of halite and fluorapatite. To adjust the simulated data to the concentrations measured in batch experiments, it was necessary to add the minerals detected by SEM/EDXS in the KINDIS simulations, and also gypsum. The comparison between rinsed and non-rinsed sample experiments showed that the precipitation of halite and gypsum from dry and wet depositions in the non-saturated zone, and subsequent leaching to the aquifer, can explain most of the chloride, sodium and sulfate sources. Nevertheless, barite is an additional source for sulfur, as it was recognized in the SEM/EDXS determinations. Regarding the usually high silica concentrations observed in the Pampean aquifer, the observed concentrations during batch experiments can be obtained from KINDIS simulations by including biogenic silica (phytoliths) as a silica source. The high concentration of fluoride could not be explained by dissolution of fluoroapatite, F-rich biotite, or trace amounts of fluoride incorporated in calcite. One of the possible sources of fluoride in water could be the desorption of this ion from the surface of other minerals.

The calibration of this geochemical kinetic code using the results of batch experiments demonstrated the importance of accessory minerals in the determination of water chemistry. Even if the solution reached a steady state composition rapidly and the use of the equilibrium concept in groundwater is correct, this kinetic approach is a valuable way to unravel the origin of the water chemistry. The KINDIS software is easy to use as the parameters can be modified easily and can be applied in the study of various types of aquifers in Argentina and in the world.

Acknowledgements

The authors are thankful to the National Agency for Science and Technology Promotion (ANPCyT, PICT 2014 N°1529) which supported this study financially and to the National Scientific and Technical Research Council (CONICET) PIP2011-0392. We also acknowledge the Mincyt-ECOS project for supporting international collaboration between the ICGyC/IIMyC in Argentina and the LHyGeS in France. The authors are also thankful to Mr. G. Bernava for chemical analysis, Amelie Aubert (LHyGES) for X-ray diffraction analyses and Gilles Morvan for SEM/EDXS analyses. The careful reviews and constructive comments by anonymous reviewers were also much appreciated for helping to improve the manuscript.

References

Al Rawahi, W., Marcilla, A.L., Ward, N.I., 2015. Arsenic Speciation Anallysis of Ground Waters in Southern La Pampa and Buenos Aires Provinces, Argentina.

Alarcón-Herrera, M.T., Bundschuh, J., Nath, B., Nicolli, H.B., Gutierrez, M., Reyes-Gomez, V.M., Sracek, O., 2013. Co-occurrence of arsenic and fluoride in groundwater of semi-arid regions in Latin America: genesis, mobility and remediation. J. Hazard. Mater. 262, 960–969.

Antoniou, E.A., Stuyfzand, P.J., van Breukelen, B.M., 2013. Reactive transport modeling of an aquifer storage and recovery (ASR) pilot to assess long-term water quality improvements and potential solutions. Appl. Geochem. 35, 173–186 (August 2013).

Bhattacharya, P., Claesson, M., Bundschuh, J., Sracek, O., Fagerberg, J., Jacks, G., ... Thir, J.M., 2006. Distribution and mobility of arsenic in the Rio Dulce alluvial aquifers in Santiago del Estero Province, Argentina. Sci. Total Environ. 358 (1), 97–120.

Borgnino, L., Garcia, M.G., Bia, G., Stupar, Y., Le Coustumer, P., Depetris, P.J., 2013. Mechanisms of fluoride release in sediments of Argentina's central region. Sci. Total Environ. 443, 245–255.

Borrelli, N., Osterrieth, M., Marcovecchio, J., 2008. Interrelations of vegetal cover, silicophytolith content and pedogenesis of typical Argiudolls of the Pampean plain, Argentina. Catena 75 (2), 146–153.

Borrelli, N., Alvarez, M.F., Osterrieth, M.L., Marcovecchio, J.E., 2010. Silica content in soil solution and its relation with phytolith weathering and silica biogeochemical cycle in typical Argiudolls of the Pampean plain, Argentina—a preliminary study. J. Soils Sediments 106, 983–994.

Bullen, T.D., Krabbenhoft, D.P., Kendall, C., 1996. Kinetic and mineralogic controls on the evolution of groundwater chemistry and 87Sr/86Sr in a sandy silicate aquifer, northern Wisconsin, USA. Geochim. Cosmochim. Acta 60 (10), 1807–1821.

Bundschuh, J., Farias, B., Martin, R., Storniolo, A., Bhattacharya, P., Cortes, J., ... Albouy, R., 2004. Groundwater arsenic in the Chaco-Pampean plain, Argentina: case study from robles county, Santiago del Estero province. Appl. Geochem. 19 (2), 231–243.

Bureau de Recherches Géologiques et Minières (BRGM) Thermochemical and Mineralogical Tables for Geochemical Modeling. Retrieved from: http://thermoddem.brgm.fr.

Calvi, C., Martinez, D., Dapeña, C., Gutheim, F., 2016. Abundanceand distribution of fluoride concentrations in groundwater: la Ballenera catchment. Southeast of Buenos Aires Province. Argentina. Environ. Earth Sci. 756, 1–12.

Chen, H., Zhan, H., et al., 2005. Sorption kinetics of naphthalene and phenanthrene in loess soils. Environ. Geol. 47, 467.

Cury, J.A., Garcia, M.G., Buzalaf, M.A.R., Akman, S., Men, Y., Rigalli, A., ... Emekli-Alturfan, E., 2015. Fluorine: Chemistry, Analysis, Function and Effects. Royal Society of Chemistry.

Dangavs, N., Blasi, A., 2002. Los depósitos de yeso intrasedimentario del arroyo El Siasgo,partidos de Monte y General Paz, Provincia de Buenos Aires. Rev. Asoc. Geol. Argent. 57 (3), 315–327.

Daval, D., Martinez, I., Guigner, J.M., Hellmann, R., Corvisier, J., Findling, N., Dominici, C., Goffe, B., Guyot, F., 2009. Mechanism of wollastonite carbonation deduced from micro- to nanometer length scale observations. Am. Minerol. 94, 1707–1726.

Di Rienzo, J.A., Casanoves, F., Balzarini, M.G., Gonzalez, L., Tablada, M., Robledo, Y.C., 2011. InfoStat versión 2011. 8. Grupo InfoStat, FCA, Universidad Nacional de Córdoba, Argentina, pp. 195–199(URL http://www.infostat.com.ar).

Dietrich, S., Bea, S.A., Weinzettel, P., Torres, E., Ayora, C., 2016. Occurrence and distribution of arsenic in the sediments of a carbonate-rich unsaturated zone. Environ. Earth Sci. 75 (2), 90.

Downs, R.T., Hall-Wallace, M., 2003. The American mineralogist crystal structure database. Am. Mineral. 88, 247–250.

Fagerlund, G., 1973. Determination of specific surface by the BET method. Mater. Constr. 6 (3), 239–245.

Farías, S.S., Casa, V.A., Vázquez, C., Ferpozzi, L., Pucci, G.N., Cohen, I.M., 2003. Naturalcontamination with arsenic and other trace elements in ground waters of Argentine Pampean Plain. Sci. Total Environ. 3091, 187–199.

Fraysse, F., Pokrovsky, O.S., Schott, J., Meunier, J.D., 2009. Surfacechemistry and reactivity of plant phytoliths in aqueous solutions. Chem. Geol. 2583, 197–206.

Frenguelli, J., 1956. Rasgos generales de la hidrografía de la Provincia de Buenos Aires LEMIT II 1956. pp. 1–19.

Garcia, M.G., Lecomte, K.L., Martínez, J.O., Formica, S.M., Depetris, P.J., 2006. Flúor en aguas de ríos de las sierras de Córdoba, Argentina. In: I Congreso Internacional sobre gestión y tratamiento integral del agua. Córdoba, Argentina.

García, M.G., Lecomte, K.L., Stupar, Y., Formica, S.M., Barrionuevo, M., Vesco, M., Ponce, R., 2012. Geochemistryand health aspects of F-rich mountainous streams and groundwaters from sierras Pampeanas de Cordoba Argentina. Environ. Earth Sci. 652, 535–545.

García, M.G., Borgnino, L., Bia, G., Depetris, P.J., 2014. Mechanisms of arsenic and fluoride release from Chacopampean sediments (Argentina). Int. J. Environ. Health Res. 7 (1), 41–57.

Garrels, R.M., Christ, C.L., 1965. Solutions Minerals and Equilibria. Harper and Row, New York (450p.).

Glok Galli, M.G., Martínez, D.E., Kruse, E.E., Grondona, S.I., Lima, M.L., 2014. Hydrochemical and isotopic characterization of the hydrological budget of a MAB reserve: Mar Chiquita lagoon province of Buenos Aires Argentina. Environ. Earth Sci. 728, 2821–2835.

Gómez, M.L., Blarasin, M.T., Martínez, D.E., 2009. Arsenic and fluoride in a loess aquifer in the central area of Argentina. Environ. Geol. 571, 143–155.

Horwitz, W., Chichilo, P., Reynolds, H., 1970. Official Methods of Analysis of the Association of Official Analytical Chemists, 11th ed. Association of Official Analytical Chemists, Washington DC.

Huo, L., Hao, J., Liu, H., Zhao, D., 2013. Effect of water content on strontium retardation factor and distribution coefficient in Chinese loess. J. Radiol. Prot. 33 (4), 791–807 (December 2013).

Khorzinskii, D.S., 1965. The theory of systems with perfectly mobile components and processes of mineral formation. Am. J. Sci. 263, 193–205.

Kitano, Y., Okumura, M., 1973. Coprecipitation of fluoride with calcium carbonate. Geochem. J. 7 (1), 37–49.

Levien, L., Prewitt, C.T., Weidner, D.J., 1980. Structure and elastic properties of quartz at pressure P = 1 atm. Am. Mineral. 65, 920–930.

Logan, W.S., Auge, M.P., Panarello, H.O., 1999. Bicarbonate sulfate and chloride water in a shallow clastic-dominated coastal flow system Argentina. Ground Water 372, 287–295.

Madé, B., Clément, A., Fritz, B., 1994. Modelling mineral/solution interactions: the thermodynamic and kinetic code KINDISP. Comput. Geosci. 20 (9), 1347–1363.

Mangeret, A., De Windt, L., Crançon, P., 2012. Reactive transport modelling of groundwater chemistry in a chalk aquifer at the watershed scale. J. Contam. Hydrol. 138-139, 60–74 (September 2012).

Markgraf, S.A., Reeder, R.J., 1985. High-temperature structure refinements of calcite and magnesite sample: T = 24 C. Am. Mineral. 70, 590–600.

Martínez, D., Bocanegra, E., 2002. Hydrogeochemistry and cation-exchange processes in the coastal aquifer of Mar Del Plata Argentina. Hydrogeol. J. 103, 393–408.

Martinez, D.E., Osterrieth, M.O., 2013. Hydrochemistry of an Aquifer in Quaternary Loess like Sediments in the Pampean Plain Argentina Revista Facultad de Ingeniería de la Universidadde Antioquia Colombia. vol 66. pp. 9–23 (ISSN 0120-6230).

Martinez, D.E., Londono, O.Q., Massone, H.E., Buitrago, P.P., Lima, L., 2012. Hydrogeochemistry of fluoride in the Quequen river basin: natural pollutants distribution in the Argentine pampa. Environ. Earth Sci. 652, 411–420.

Martinez, D.E., Moschione, E., Bocanegra, E., Glok Galli, M., Aravena, R., 2014. Distribution and origin of nitrate in groundwater in an urban and suburban aquifer in Mar del Plata Argentina. Environ. Earth Sci. 72 (6), 1877–1886.

Martínez, D.E., Fourré, E., Londoño, O.Q., Jean-Baptiste, P., Glok Galli, M.G., Dapoigny, A., Grondona, S.I., 2016. Residence time distribution in a large unconfined–semiconfined aquifer in the Argentine Pampas using 3H/3He and CFC tracers. Hydrogeol. J. 1–14.

Meyling, A.H., Meyling, J., 1963. Analyst 88, 84.

Miretzky, P., Conzonno, V., Cirelli, A.F., 2001. Geochemical processes controlling silica concentrations in groundwaters of the Salado River drainage basin Argentina. J. Geochem. Explor. 733, 155–166.

Nadler, A., Magartiz, M., Mazor, M., 1980. Kinetics of chemical processes in a carbonate aquifer: a case study of water-rock interaction in the aquifer of western and central Galilee (Israel). J. Hydrol. 45 (1–2), 39–56.

Nicolli, H., Suriano, J., Gomez Peral, M., Ferpozzi, L., 1989. Groundwater Contamination with Arsenic and other trace elements in an area of the Pampa Province of Córdoba Argentina. Environ. Geol. Water Sci. 141, 3–16.

Nicolli, H.B., Bundschuh, J., Blanco, M.D., Tujchneider, O.C., Panarello, H.O., Dapena, C., Rusansky, J.E., 2012. Arsenic and associated trace-elements in groundwater from the Chaco-Pampean plain Argentina: results from 100years of research. Sci. Total Environ. 429, 36–56 (2012 Jul 1).

Oelkers, E.H., Schott, J., 1995. Experimental study of anorthite dissolution and the relative mechanism of feldspar hydrolysis. Geochim. Cosmochim. Acta 5924, 5039–5053.

Osterrieth, M.L., Martínez, G.A., 1993. Paleosols on late Cainozoic loessic sequences in the northeastern side of Tandilia range, buenos aires, Argentina. Quat. Int. 17, 57–65.

Osterrieth, M., Benvenuto, L., Alvarez, M., Honaine, M., 2014. Silicophytoliths: Relevant buffer in the process of weathering of Typic Argiudolls, Argentinean Pampean plains 9th International Meeting for Phytolith Research: Toward Integrative Phytolith Research Abstracts, International Phytolith Society, Brusselspp 42–43.

Osterrieth, M., Borrelli, N., Alvarez, M.F., Honaine, M.F., 2015. Silica biogeochemical cycle in temperate ecosystems of the Pampean plain, Argentina. J. S. Am. Earth Sci. 63, 172–179.

Palandri, J.L., Kharaka, Y.K., 2004. A Compilation of Rate Parameters of Water-Mineral Interaction Kinetics for Application to Geochemical Modeling. Geological Survey, Menlo Park CA.

Pérez-Carrera, A., Cirelli, A.F., 2010. Arsenic and Water Quality Challenges in South America in Water and Sustainability in Arid Regions. Springer, Netherlands, pp. 275–293.

Prewitt, C.T., Sueno, S., Papike, J.J., 1976. The crystal structures of high albite and monalbite at high temperatures T = 24 deg C. Am. Mineral. 61, 1213–1225.

Pye, K., 1995. The nature, origin and accumulation of loess. Quat. Sci. Rev., 14 7–8., pp. 653–667.
Quiroz Londoño, O.M., Martínez, D.E., Dapeña, C., Massone, H., 2008. Hydrogeochemistry and isotope analyses used to determine groundwater recharge and flow in low-gradient catchments of the province of Buenos Aires Argentina. Hydrogeol. J. 166, 1113–1127.
Quiroz Londoño, O.M., Martinez, D.E., Massone, H.E., 2012. Comparative assessment of recharge estimation methods in plain environments. The inter-mountainous plain (Argentina) as a case study. Dyna 79 (171), 239–247.
Rodríguez-Carvajal, J., 2001. Recent developments of the program FULLPROF. Commission on powder diffraction IUCr. Newsletter 26, 12–19.
Schultz, C., Castro, E., 2003. Estudio planificación y explotación del agua subterránea. Una trilogía utópica en la República Argentina. III Congreso Argentino de Hidrogeología. Actas I. pp. 219–225 (Rosario, Argentina).
Smedley, P.L., Nicolli, H.B., Macdonald, D.M.J., Barros, A.J., Tullio, J.O., 2002. Hydrogeochemistryof arsenic and other inorganic constituents in groundwaters from La Pampa Argentina. Appl. Geochem. 173, 259–284.
Tabatabai, M.A., 1974. A rapid method for determination of sulfate in water samples. Environ. Lett. 73, 237–243.
Teruggi, M.E., 1957. The nature and origin of Argentine loess. J. Sediment. Res. 273.
Tricart, J., 1973. Geomorfología de la Pampa Deprimida: base para los estudios edafológicos y agronómicos; Plan Mapa de Suelos de la Región Pampeana Secretaría de Estado de Agricultura y Ganadería de la Nación Inst Nacional de Tecnología Agropecuaria INTA.
Vital, M., Martínez, D.E., Borrelli, N., Quiroga, S., 2015. Kineticsof dissolution processes in loess-like sediments and carbonate concretions in the southeast of the province of Buenos Aires Argentina. Environ. Earth Sci.
Zabala, M.E., Manzano, M., Vives, L., 2015. The Origin of Groundwater Composition in the Pampean Aquifer Underlying the del Azul Creek Basin Argentina. Sci. Total Environ. 518, 168–188.
Zhu, C., 2005. In situ feldspar dissolution rates in an aquifer. Geochim. Cosmochim. Acta 69 (6), 1435–1453.
Zhu, C., Veblen, D.R., Blum, A.E., Chipera, S.J., 2006. Naturally weathered feldspar surfaces in the Navajo sandstone aquifer, black mesa, Arizona: electron microscopic characterization. Geochim. Cosmochim. Acta 70 (18), 4600–4616.